FLUID-STRUCTURE INTERACTION (FSI) SIMULATIONS ON THE SENSITIVITY OF CORIOLIS FLOW METER UNDER LOW REYNOLDS NUMBER FLOWS

Vivek Kumar, Martin Anklin, Benjamin Schwenter*[1]
Research and Development, Endress+Hauser Flowtec AG, Kaegen Str. 7, Reinach (BL) CH-4132, Switzerland
Phone:+41-61-715 6976, FAX:+41 61-715 6891, E-mail:vivek.kumar@flowtec.endress.com

Abstract: In process industries Coriolis mass flow meters (CMFs) are widely employed for measuring mass flow rates. Quite often especially in oil and gas (O&G) industry, owing to fluids with high viscosities, flow measurements may lie in low Reynolds number regions. At low Reynolds numbers (Re), a CMF reading may deviate under the influence of fluid-dynamic forces. With the help of extensive Fluid-Structure-Interaction simulations (FSI), a detailed insight into physical mechanisms leading to this deviation is provided. The main finding is that this deviation is a function of the Reynolds number and the effect can be explained by a periodic shear mechanism which interacts with the oscillatory Coriolis force. Experimental results with and without the correction are shown and compared with corresponding numerical results.

Keywords: Coriolis mass flow (CMF) meter, FSI Simulations, Reynolds number

1. Introduction

Advancements and developments in the field of computational sciences in the past have led to extensive use of numerical methods in engineering. Unlike a few years ago, now computational fluid dynamics (CFD) and computational structural mechanics (CSM) find plenty of applications and interests in non-conventional, other than aero-space, turbomachinery, industries. The flow measurement industry is one of such examples where application of these numerical tools is helping to improve product quality and to find innovative solutions. In flow measurement devices, especially a Coriolis flow meter, fluid-structure interaction (FSI), i.e. where CSM and CFD need to be coupled, related problems are often encountered and a complete understanding of physical phenomena occurring in devices becomes vital.
These days, coupling between CSM and CFD is offered by a few commercial programs in the market. ANSYS's fluid-structure interaction module is one of such tools which helps us to simulate thermal and mechanical fluid-structure interaction effects in various flow measurement devices. In this work, application of the FSI simulations on studying low Reynolds number effects in a CMF is presented.

Coriolis mass flow meters are nowadays widely utilized in process industry due to their high accuracy, reliability and direct measurement of mass flow rate and fluid density in continuous and batch processes. In a CMF, the phase difference between two sensor points across the center of the oscillating tube is directly proportional to the mass flow rate in the tube. The proportionality constant between mass flow and the phase difference is referred as the calibration factor of the meter. The phase difference is measured with an electro-magnetic inductive sensor

[1] M.Sc. Student ETH Zurich Switzerland

during a measurement and further utilized to calculate the mass flux and flow rate in the meter. A 2-inch CMF from Endress+Hauser (E+H) Flowtec AG is shown in Figure 1. Under certain conditions, a meter may deviate from this linear behaviour depending on the process conditions in the measuring line. These disturbances are mainly due to coupled dynamics of fluid and structure. Typical examples of disturbances are e.g. change in the compressibility of the fluid, presence of air-bubbles, line pressure and extreme low Reynolds number flows.

Figure 1: Promass F DN50, the two-inch Coriolis mass flow meter of E+H Flowtec AG.

In the present study, the focus is given to possible mechanisms leading to deviation in meter reading from high to low Reynolds number regions. The measurement deviation at low Re number has significant importance in the metering of high viscous fluids. Several laboratory and field measurements with certain devices clearly indicate that there can be a shift in the meter calibration factor at low Reynolds numbers. A typical deviation starts at Re=10'000 [see Eq. (9)] and the maximum deviation is approximately 0.5 to 1% at about Re = 800. The Reynolds number effect for a 6-inch E+H Flowtec AG device Promass F DN150 is shown in Figure 1 below. Both corrected and uncorrected measured data are presented in the figure.

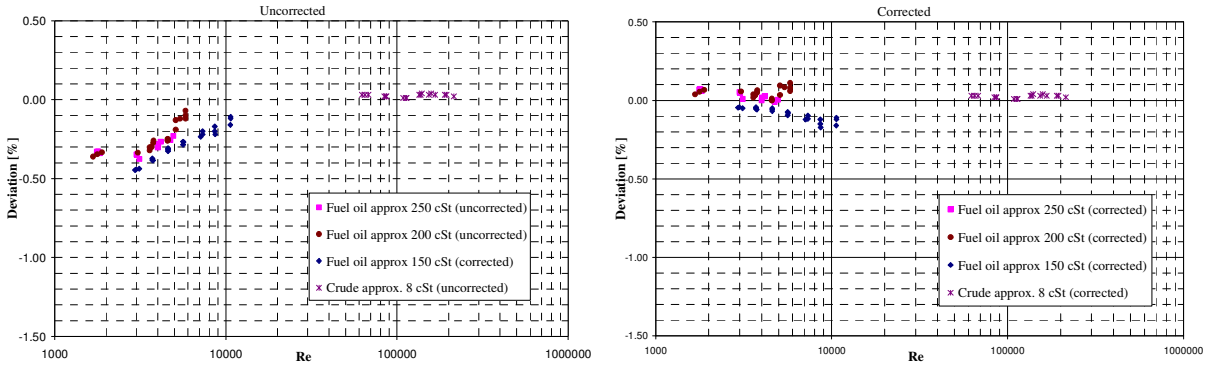

(a) Uncorrected values (b) Online corrected values

Figure 2: A shift in the meter reading with decreasing Reynolds number indicating the presence of a fluid dynamic phenomenon responsible behind the shift.

The effect shown in Figure 2(a) is explored with the help of present numerical simulations. In the mass flow meters of E+H Flowtec AG a compensation algorithm is implemented in the signal processing device in order to correct this deviation online. The measurement data after the online correction is presented in Figure 2(b). It may be noticed the compensation without any additional calibration works well.

As far as Coriolis flow meters are concerned, there are a few attempts to simulate a CMF using coupled FSI approach [1-3]. Kutin et al.[1-3] coupled the finite-element Abacus and finite-volume Comet program mainly to investigate flow profile effects in straight-tube Coriolis meters. According to Kutin et al., the present effect is due to the change in axial flow profile due to the variation in the Reynolds number. Kutin et al. [3] attributed the shift in meter readings with respect to decreasing Reynolds numbers to the change in axial flow profiles from turbulent to laminar transitions.
The present investigations with the help of numerical simulations suggest that a periodic or time-dependent mechanism arising due to the interaction of oscillating inertial and oscillating shear force give rise to the shift in the meter reading of a CMF. The ratio of the two oscillating forces is directly proportional to the Reynolds number of the mean flow.

2. Mathematical Modeling

The working of a Coriolis meter involves the mesh or boundary movement on both structure and fluid sides. The movement of the oscillating tubes is superimposed on the flowing-fluid which in response exerts a force on the structure due to its inertia. The inertial force of the fluid leads to a change in the oscillation behaviour of the structure is recorded in terms of displacements. In this section, we briefly present the governing equations and corresponding general boundary/initial conditions which we have utilized in the present simulations.

2.1. Fluid Domain

For the fluid side the governing equations are transformed to Arbitrary Lagrangian-Eulerian (ALE) form in order to account for the convective fluxes which are resulted due to the mesh movement. The conservation equations of mass and momentum in integral form for the present simulations:

$$\frac{d}{dt}\int_{\Delta V}\rho_f \, dV + \int_{\Delta S}\rho_f \,(U_i - u_i^s)\, dS_i = 0 \tag{1}$$

$$\frac{d}{dt}\int_{\Delta V}\rho_f \, U_j \, dV + \int_{\Delta S}\rho_f \,(U_i - u_i^s) U_j \, dS_i = \int_{\Delta S}(\tau_{ij} + \tau_{ij}^T - P\,\delta_{ij})\, dS_i \tag{2}$$

where ρ_f denotes the density of fluid, U_j is the fluid velocity vector, u_i^s the velocity of the mesh due to structural motion, τ_{ij} and τ_{ij}^T are the viscous and turbulent part of the momentum transport tensors, respectively, P represents the fluid pressure, S_i denotes the surface-area vector and V the volume of the control-volume. The turbulent shear-stress tensor is given by eddy-viscosity hypothesis and the eddy-viscosity was modelled by the standard $k-\varepsilon$ turbulence model for turbulent flows.

For the fluid domain, standard inlet and outlet boundary conditions (BCs) were utilized where on the inlet patch fully-developed flow profile is prescribed. Both inlet and outlet BCs were kept away from the FSI-surface to minimize the influence of BCs errors on the simulation results. For turbulent quantities i.e. k and ε zero-gradient boundary conditions were used at the outlet. At the fluid-structure interface or oscillating tube-wall the no-slip boundary was specified and an implicit mesh motion was imposed which was provided by the CSM solver. A typical structural mapped numerical mesh used in the FSI simulations is presented in Figure 3. The height of the cell next to the oscillating wall was determined on the basis of thickness of Reynolds and Stokes layers [5].

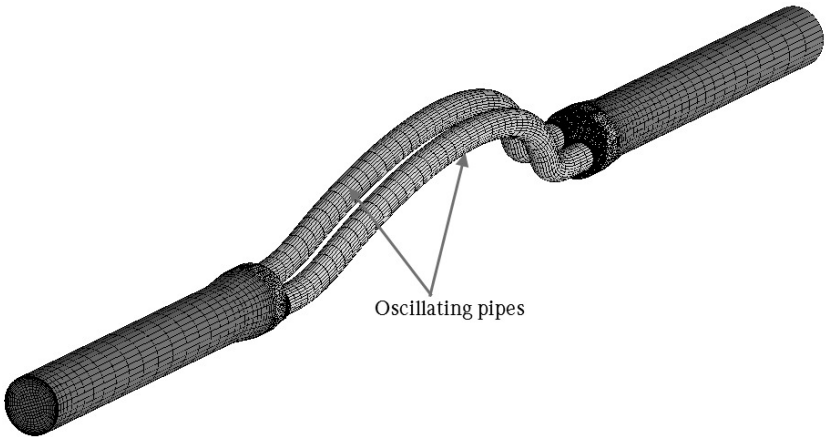

Figure 3: A typical block-structured numerical mesh used for FSI simulations for 2-inch Promass F.

2.2. Solid Domain

In all computations in the present work, the structure was assumed to be a linear elastic structure and the differential form of equation of motion for a linear elastic structure may be written as:

$$\frac{\partial^2 \rho_s \phi_j}{\partial t^2} = \frac{\partial \tau_{ij}^s}{\partial x_i} + \rho_s b_j \tag{3}$$

where ϕ_j represents structural displacement vector, ρ_s the solid density, t the time, b_j the body-force acting on a structure. Here, τ_{ij}^s represents the stress tensor and can be written as:

$$\tau_{ij}^s = \mu_s \left(\frac{\partial \phi_j}{\partial x_i} + \frac{\partial \phi_i}{\partial x_j} \right) + \lambda_s \frac{\partial \phi_k}{\partial x_k} \delta_{ij} \tag{4}$$

where μ_s and λ_s are Lame's coefficient and are related to Young's modulus of elasticity E and Poisson ratio ν_s as follows:

$$\mu_s = \frac{E}{2(1+\nu_s)} \tag{5}$$

and

$$\lambda_s = \frac{\nu_s E}{(1+\nu_s)(1-2\nu_s)} \tag{6}$$

For the structural-side boundary conditions, the solid-tube was always kept fixed at both ends. In order to simulate the tube exciter, a periodic or harmonic force was applied at the center of tube only for the first cycle. The frequency of the oscillating force was set equal to the first eigen-frequency of the pipe or the drive frequency of the meter. For pipe oscillations in x-direction, a periodic was applied at the center in order to simulate the function of an exciter:

$$b_j = \begin{cases} [b_0 \sin(2\pi n f_d \Delta t), 0, 0] & \text{if } n \le 20, \\ [0,0,0] & \text{else} \end{cases} \tag{7}$$

here Δt is the integration time step, f_d denotes the drive frequency, and b_0 represents the amplitude of the periodic force. The coupled simulations are performed until the amplitude of the oscillations goes below a certain value.

The structural domain and numerical mesh is shown in Figure 4. It may be seen that the distribution of cell on the structural mesh and fluid mesh are not identical. The interface quantities were transferred across the fluid-solid interface in every iteration.

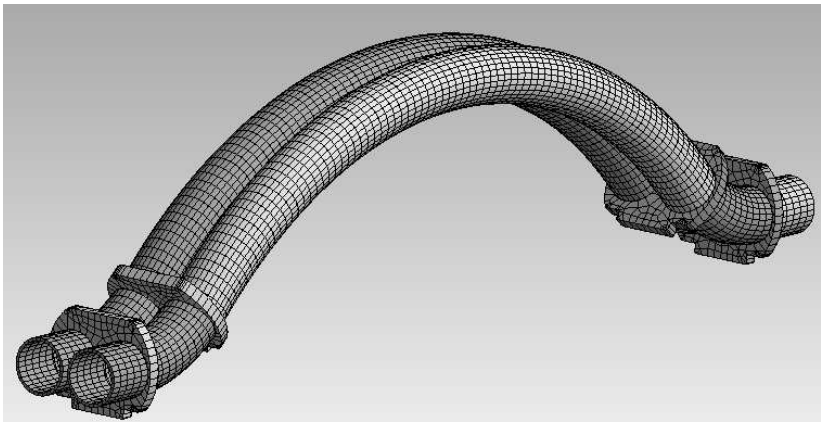

Figure 4: The structural mapped mesh for solid domain.

2.3. CFD-FEM Coupling Approach

The solution approach in a FSI computation is a critical factor for the convergence of stagger iterations. Before the start of the transient simulations, separate initial computations were performed on the fluid and on the structure side. On the structure side, a modal (or eigen) analysis was performed to find out the drive frequency (f_d) of the meter. On the fluid side, a steady-state simulation was carried out to initialize the flow and pressure fields on the fluid side. As a next step, fluid and structure fields were coupled and a single steady-state simulation was performed to achieve reasonable initial fields on the fluid and the structure side. The size of the time-step was estimated by dividing the each cycle of the pipe oscillations in 20-steps. This temporal resolution was found to be appropriate for reasonable predictions. For the FSI coupling, the following information is transferred between the fluid-structure interface:

$$\begin{aligned} U_i\big|_s &= U_i\big|_l \\ \phi_i\big|_s &= \phi_i\big|_l \\ F_j^{FSI} &= \int (P\,\delta_{ij} + \tau_{ij} + \tau_{ij}^T)\, dS_i^{FSI} \end{aligned} \tag{8}$$

The above boundary conditions set both kinematic and dynamic constraints for the FSI interface, where F_j^{FSI} denotes the total force vector from the fluid solver to the structural solver. On the other hand, structural displacements ϕ_i were transferred from the structure to the fluid in order to fulfill kinematic constraints.

The entire FSI simulation was run over 12-15 periods or approximately 300 time-steps and the displacements at two sensor-locations were recorded at each time-step. For a typical case, a computing time of approximately 60 CPU hours is required for fully converged solution for 15 periods. Consequently the phase difference between two sensor locations was found out with the help of a signal processing tool. A typical signal displacement and the corresponding phase difference at a given flow 3.3m/s flow speed in the measuring tubes is shown in the figure below

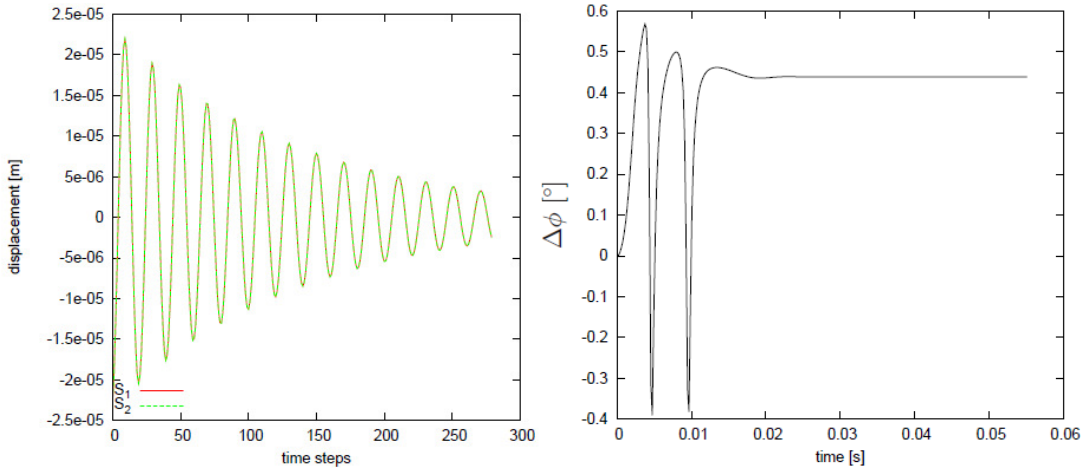

(a) (b)

Figure 5: Recorded sensor signal at two sensor points (a) and corresponding phase difference (b) for the Promass sensor from E+H.

3. Results and Discussions

3.1. Reynolds Number Effect

As mentioned in an earlier section, the calibration constant of a Coriolis mass flow meter may shift at low Reynolds number. The Reynolds number in the measuring tube is calculated as

$$\mathrm{Re} = \frac{4\dot{m}}{n_t \pi \mu d} \qquad (9)$$

where $\dot{m}$ is the mass flow rate, n_t the number of measuring tubes, μ the dynamic viscosity and d denotes the inner diameter of the measuring tube.

In the present section we try to elucidate the mechanism which is behind this shift. With the help of coupled FSI simulations, influence of Reynolds number is simulated and numerical computed phase difference values are compared with the experimental data of the same device. From Figure 6 it may be noticed that the numerical simulations qualitatively support the experimental observations.

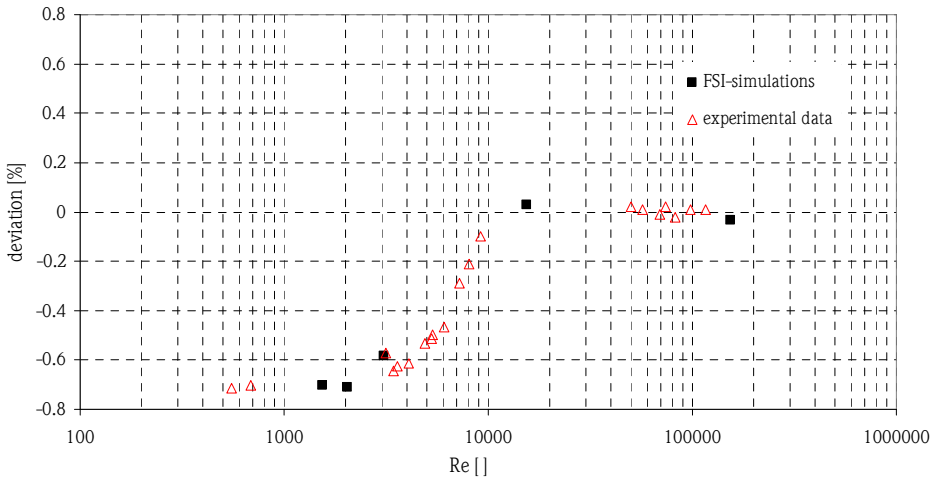

Figure 6: A comparison between experimental and numerical simulation results indicating a shift in meter calibration factor in low Reynolds number region.

Now the question arises what exactly is behind this shift in the meter response. In order to understand this mechanism, following the Reynolds decomposition the fluid flow equations are split [4] into two parts: steady component and oscillating or first harmonic component such that

$$\begin{aligned} U_j &= \overline{U}_j + u_j' \\ P &= \overline{P} + p' \\ \tau_{ij} &= \overline{\tau}_{ij} + \sigma_{ij} \end{aligned} \tag{10}$$

where quantities with overbar are the mean or time independent quantities and superscript " ' " indicates oscillating or periodic quantities. The oscillating quantities are only a function of drive frequency and time, and influence of high order harmonics e.g. from turbulence and structure dynamics can be neglected for the case of a Coriolis meter. The higher order harmonics and fluctuations are anyway filtered out by the digital signal processing device and therefore in general do not contribute to the meter readings.

By employing the above definitions one may split velocity, pressure and shear-stress terms in the Navier-Stokes equations into steady and oscillating parts in order to derive equations from oscillating velocity fields. Consequently, with the help of a few mathematical operations and neglecting the non-linear oscillating term, that is $\rho u_i' u_j'$, the momentum balance for the oscillating flow in the differential form can be written as:

$$\frac{\partial \rho u_j'}{\partial t} + \underbrace{\left(\frac{\partial \rho u_j' \overline{U}_i}{\partial x_i} + \frac{\partial \rho u_i' \overline{U}_j}{\partial x_i} \right)}_{\text{oscillating Coriolis force term}} = -\frac{\partial p'}{\partial x_i}\delta_{ij} + \underbrace{\frac{\partial \sigma_{ij}}{\partial x_i}}_{\text{oscillating shear force term}} \tag{11}$$

With the help of post-processing tools, the quantities: oscillating force and corresponding shear-rate are integrated over the tube cross-section at sensor location and plotted in Figure 7 against the Reynolds number. It is interesting to note that both inertial force and shear in the tube cross-section closely follow the meter deviation. Therefore one may conclude that the shear rate $\partial u_j' / \partial x_i$ contributes to the change in the Coriolis force and hence it alters the calibration factor as well.

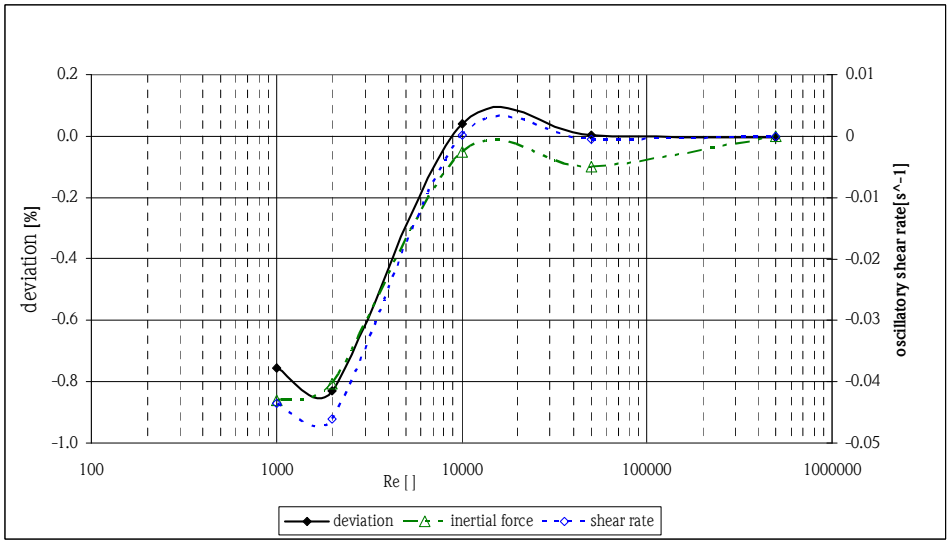

Figure 7: A deviation in the meter reading with Reynolds number and corresponding volume-averaged Coriolis or inertial force, $\int \frac{\partial \rho u_j' \overline{U}_i}{\partial x_i} dV$, and shear rate $\frac{\partial u_j'}{\partial x_i}$.

The interaction of the oscillatory shear force with the inertial force in the measuring tube gives rise to an oscillatory secondary flow. At a given time, this secondary flow moves in opposite directions in either sides of the tube center and disappears at the center of the tube. The secondary flow at a Reynolds number of 100 is shown in Figure 8(a). At sufficiently high Reynolds number this secondary flow disappears and consequently the ratio of shear force to Coriolis force becomes negligibly small.

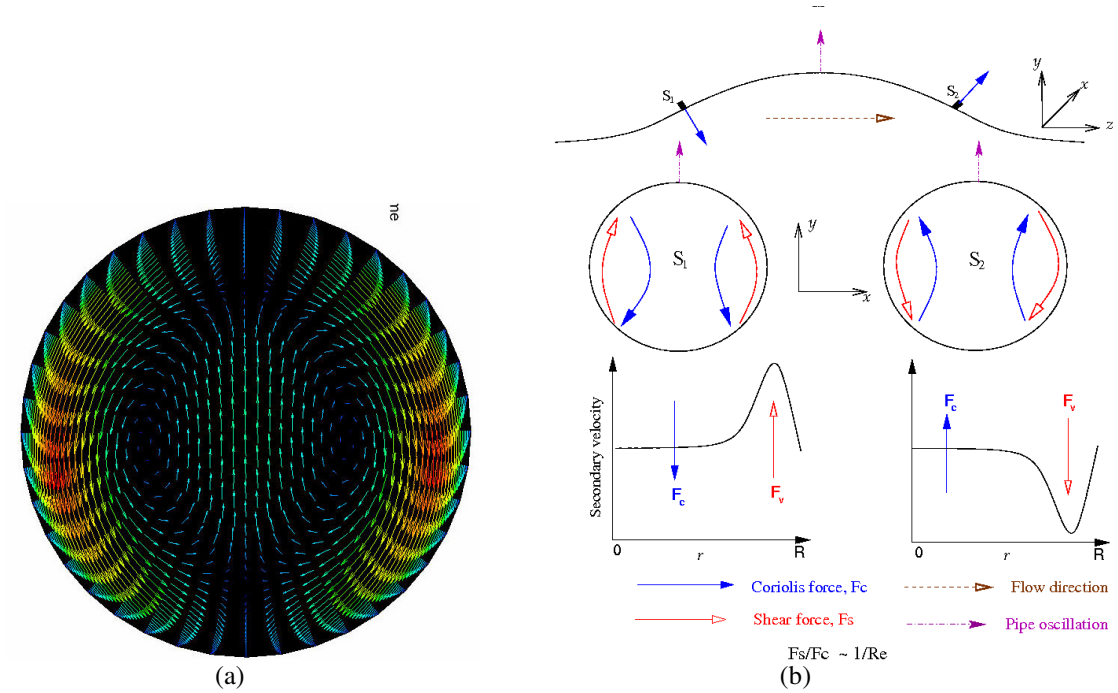

(a) (b)

Figure 8: (a) The computed oscillatory secondary flow in moving-frame of reference at the position where sensor is located, (b) a schematic representation of the oscillatory mechanism responsible for Reynolds effect.

The understanding of the proposed mechanism behind the Reynolds number effect is achieved with the help of Fluid Structure Interaction (FSI) simulation. The phenomenon behind is briefly described with the help of a schematic diagram in Figure 8. As shown in the figure, the Coriolis force interacting with the shear force induces an asymmetric force in the measuring tube. The lower two panels illustrate that the Coriolis force induces a shear layer indicating a secondary circulation in the cross-section of the measuring tube. The Coriolis force has to overcome the shear force and part of the energy of the Coriolis force is dissipated in the secondary circulation and does not contribute to the deflection of the tube. This explains why the meter reading is below the actual mass flow. The magnitude of the secondary circulation is strongly decreasing with higher Reynolds numbers as the thickness of the shear-layer decreases exponentially with the increasing Reynolds number. Consequently, the effect becomes insignificant above a certain Reynolds number.

3.2. Real time Correction for the Low-Re Effect

In order to meet accuracy requirements in low-Re applications, the Reynolds number effect must be compensated. If it comes to meet the accuracy requirements for certain applications e.g. custody transfer, calibrations of meters is advisable for meters that are used in the low Reynolds number range, i.e. with high viscous products [6].

If a Coriolis meter has the ability of deriving a measure for viscosity directly, compensation can be done on-line by on-board means. The E+H Flowtec CMF meters can measure mass flow and fluid viscosities in real time and hence the correction for the effect is performed directly in the electronics. The following figures show that such compensation methods can be applied with a good accuracy in the device. The present correction works well with an uncertainty of $\pm 0.2\%$ without additional calibrations as can clearly be observed from Figure 9 (b).

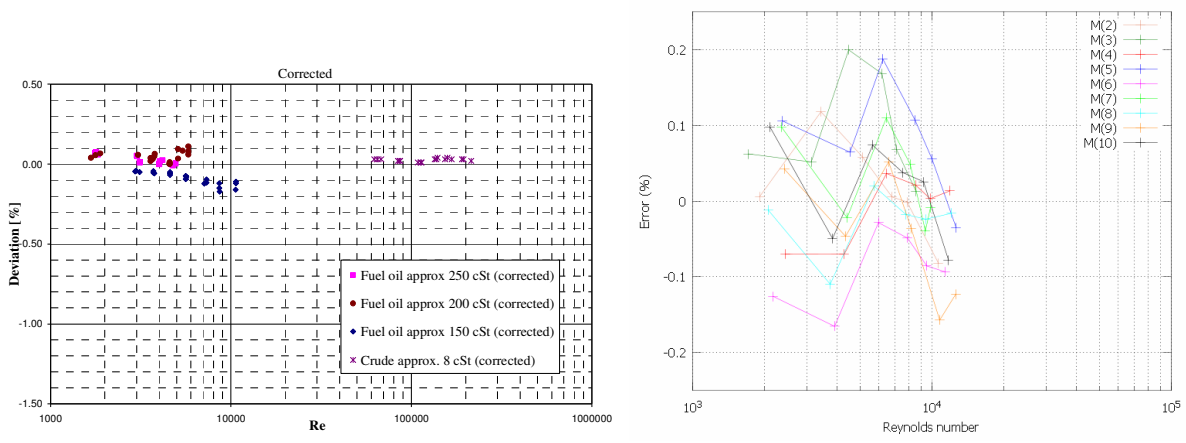

(a) (b)

Figure 9: The response of an E+H Flowtec AG Re-correction (a) for a 6-inch meter and (b) six 10-inch meters at a flow calibration facility of SPSE in southern France.

It is important to mention that this correction is implanted in the signal processing device of E+H devices and moreover the procedure is patented by E+H Flowtec.

4. Conclusion

In this work results from coupled fluid-structure numerical simulations mainly for low Reynolds numbers are presented. With the help of these simulations the fluid dynamic effect responsible for the meter deviation at low Reynolds numbers is well understood. A secondary oscillatory flow in the tube cross-section, induced by the interaction of Coriolis and shear forces, gives rise to change in the calibration factor of the meter. The secondary flow is function of the Reynolds number of the mean flow.

Since Coriolis meters of E+H Flowtec can determine the Reynolds number directly, a real time Reynolds correction is implemented in the signal processing tool in order to compensate the effect. It has been shown that the online compensation with the standard procedure works well. In general, all Coriolis devices are subjected to the Reynolds number effect and for high accuracies the effect must be compensated. In the low Re regime, the compensation algorithm is already implemented in the electronics of all E+H Coriolis meters.

List of Symbols

Abbreviations

BC	boundary condition
CFD	computational fluid dynamics
CMF	Coriolis mass flow meter
CSM	computation structural mechanics
FSI	fluid-structure interaction
Re	Reynolds number
E+H	Endress & Hauser

Roman letters

b_j	body force
d	measuring tube inner diameter
f_d	drive frequency
F_i	Force exerted by fluid
$\dot{m}$	Mass flow rate
n	n-th time-step
n_t	number of tubes
$P, \overline{P}$	pressure, time-averaged pressure
p'	oscillating pressure
S_i	surface area vector
t	time
$U_i, \overline{U}_i$	fluid velocity vector, time-averaged velocity
u_i^s	structural velocity vector
u_i'	oscillating velocity vector
U_t	mean flow speed in the measuring tube
V	volume
x_i	spatial coordinate vector

Greek letters

δ_{ij}	2nd order unit tensor
ϕ_j	displacement vector
μ	dynamic viscosity
μ_s, λ_s	Lame's coefficients
ν_s	Poisson ratio
ρ_f	Fluid density
ρ_s	Solid density
σ_{ij}	oscillating or filtered part of the viscous stress tensor
τ_{ij}	viscous stress tensor
τ_{ij}^T	turbulence stress tensor

References

[1] J. Kutin, J. Hemp, G. Bobovnik, and I. Bajsi´c. Weight vector study of velocity profile effects in straight-tube Coriolis flow meters employing different circumferential modes. Flow Measurement and Instrumentation, 16:375–385, 2005.

[2] Bobovnik G., Mole N., J. Kutin, B. Stok, and I Bajsi´c. Coupled finite-volume/finite element modeling of the straight-tube Coriolis flow meter. Journal of Fluid and Structures, pages 785–800, 2005.

[3] J. Kutin, G. Bobovnik, J. Hemp, and I. Bajsic. Velocity profile effects in Coriolis mass flow meters: Recent findings and open questions. Flow Measurement and Instrumentation, 17:349–358, 2006.

[4] O. Reynolds, On the dynamical theory of incompressible viscous fluids and determination of the criterion, Philos. Trans. of R. Soc. London, Ser A-186, pp-123-164, 1895

[5] H. Schlichting, K. Gersten, Boundary Layer Theory, 8th Edition, Springer-Verlag 2000.

[6] V. Kumar, P. Tschabold, M: Anklin, Influence and Compensation of Process Parameters on Coriolis Meters with a View to Custody Transfer of Hydrocarbon Products, NEL 9th South East Asia Hydrocarbon Flow Measurement Workshop, March 2010.